



Transcriptomic analysis of intracellular RNA granules and small extracellular vesicles: Unmasking their overlap in a cell model of Huntington's disease

Deepti Kailash Nabariya^a, Lisa Maria Knüpfer^a, Patrick Hartwich^b, Manuela S. Killian^b, Florian Centler^c, Sybille Krauß^{a,*}

^a Human and Neurobiology, Department of Chemistry and Biology, University of Siegen, Siegen, Germany

^b Chemistry and Structure of Novel Materials, Department of Chemistry and Biology, University of Siegen, Siegen, Germany

^c Bioinformatics, School of Life Sciences, University of Siegen, Siegen, Germany

ARTICLE INFO

Keywords:

Extracellular vesicles
RNA granules
Stress granules
Huntington's disease
Neurodegeneration
RNA binding proteins

ABSTRACT

Huntington's disease (HD) arises from the abnormal expansion of a CAG repeat in the *HTT* gene. The mutant CAG repeat triggers aberrant RNA-protein interactions and translates into toxic aggregate-prone polyglutamine protein. These aberrant RNA-protein interactions also seed the formation of cytoplasmic liquid-like granules, such as stress granules. Emerging evidence demonstrates that granules formed via liquid-liquid phase separation can mature into gel-like inclusions that persist within the cell and may act as precursor to aggregates that occur in patients' tissue. Thus, deregulation of RNA granules is an important component of neurodegeneration. Interestingly, both the formation of intracellular membrane-less organelles like stress granules and the secretion of small extracellular vesicles (sEVs) increase upon stress and under disease conditions. sEVs are lipid membrane-bound particles that are secreted from all cell types and may participate in the spreading of misfolded proteins and aberrant RNA-protein complexes across the central nervous system in neurodegenerative diseases like HD. In this study, we performed a comparative transcriptomic analysis of sEVs and RNA granules in an HD model. RNA granules and sEVs were isolated from an inducible HD cell model. Both sEVs and RNA granules were isolated from induced (HD) and non-induced (control) cells and analyzed by RNA sequencing. Our comparative analysis between the transcriptomics data of HD RNA granules and sEVs showed that: (I) intracellular RNA granules and extracellular RNA vesicles share content, (II) several non-coding RNAs translocate to RNA granules, and (III) the composition of RNA granules and sEVs is affected in HD cells. Our data showing common transcripts in intracellular RNA granules and extracellular sEVs suggest that formation of RNA granules and sEV loading may be related. Moreover, we found a high abundance of lncRNAs in both control and HD samples, with several transcripts under REST regulation, highlighting their potential role in HD pathogenesis and selective incorporation into sEVs. The transcriptome cargo of RNA granules or sEVs may serve as a source for diagnostic strategies. For example, disease-specific RNA-signatures of sEVs can serve as biomarker of central nervous system diseases. Therefore, we compared our dataset to transcriptomic data from HD patient sEVs in blood. However, our data suggest that the cell-type specific signature of sEV-secreted RNAs as well as their high variability may make it difficult to detect these biomarkers in blood.

1. Introduction

Huntington's disease (HD) is a hereditary neurodegenerative disorder caused by a CAG repeat expansion mutation in the Huntingtin (*HTT*) gene encoding an extended polyglutamine motif in the N-terminus of the

mutant HTT protein. Intracellular aggregates of mutant HTT protein in the patients' brains are a pathological hallmark of the disease. While the *HTT* gene is ubiquitously expressed, the expression of mutant *HTT* in the brain leads to a movement disorder with cognitive decline and behavioral abnormalities. In addition non-neuronal peripheral tissues can

This article is part of a special issue entitled: Extracellular vesicles-based theranostics published in Molecular and Cellular Probes.

* Corresponding author.

E-mail address: sybille.krauss@uni-siegen.de (S. Krauß).

<https://doi.org/10.1016/j.mcp.2025.102026>

Received 5 July 2024; Received in revised form 13 March 2025; Accepted 13 March 2025

Available online 14 March 2025

0890-8508/© 2025 The Authors. Published by Elsevier Ltd. This is an open access article under the CC BY license (<http://creativecommons.org/licenses/by/4.0/>).

show pathological changes [1].

The subcellular localization of mutant RNA is one essential aspect of disease development. Generally, RNA-binding proteins determine the functional fate of RNAs [2]. RNA-protein complexes can form spherical, membrane-less RNA granules (reviewed in [3–7]). RNA granules control processes like RNA translation, RNA transport, RNA splicing and RNA decay (reviewed in [8]). Cytoplasmic RNA granules are categorized into processing bodies (p-bodies), stress granules (SGs), and neuronal RNA transport granules.

SGs are approximately 100–200 nm in size (reviewed in [3,9,10]) and their formation is induced by different stress stimuli, for example viral infections, oxidative stress, ultraviolet (UV) radiation, hypoxia or disease-conditions (reviewed in [5]). SGs contain many RNAs and proteins including several preinitiation and translation-factors. Their primary function is to promote cell survival by condensing translationally stalled mRNAs, ribosomal components, translation initiation factors, and RNA-binding proteins (reviewed in [5]).

Initially, formation of aberrant RNA granule in HD was described for nuclear foci [11]. Later studies showed that in HD cytoplasmic SGs are also deregulated. In HD the mutant HTT protein interacts with SG-proteins and is recruited into SGs under endoplasmic reticulum (ER) stress. Moreover, SG-associated proteins are overexpressed in cortices of HD mouse models and HD patients, for example G3BP1, which initiates SG assembly via multimerization [12]. Besides the deregulation of SGs, p-body formation is affected in HD as well [13], suggesting that the intracellular dynamic system of RNA granule formation is deregulated upon expression of mutant *HTT*.

Besides this intracellular RNA sorting into granules, RNA can also be transported between cells. This intercellular transport contributes to cell-cell communication and involves extracellular vesicles (EVs). EVs can be grouped by their size into small EVs (sEVs, <200 nm in diameter, e.g., exosomes) and large EVs (lEVs >200 nm in diameter, e.g., microvesicles and apoptotic bodies) [14]. sEVs play an important role in the central nervous system, ranging from the removal of biomolecules from cells to eliminate waste to intercellular communication. sEVs originate from multivesicular endosomes and are secreted under both physiological and pathophysiological conditions. During vesiculation, proteins, lipids, and nucleic acids are encapsulated within sEVs [15]. Especially in the nervous system, sEVs contribute to cell-to-cell interaction. There is substantial evidence that EVs secreted from neurons, astrocytes, microglia, and oligodendrocytes contain different and unique sets of proteins and RNAs (reviewed in [16]). sEVs released from primary cortical neurons and astrocytes contain proteins, such as the prion protein, the L1 cell adhesion molecule, and some subunits of glutamate receptors [17]. The presence of the synapsin-I protein in the sEVs secreted from glial cells indicates their role in supporting neuronal health and axonal outgrowth [18]. sEVs released from oligodendrocytes contain myelin proteins as well as a few proteins associated with protection against cell stress [19]. Understanding the release and function of sEVs can be of immense biological interest for understanding mechanisms of cell-to-cell communication and their role in disease development. With respect to HD, mutant HTT impairs sEV secretion in astrocytes [20]. Both HTT protein and RNA are secreted via sEVs [21, 22]. Involvement of sEVs in disease transmission was demonstrated in models where human sEV carrying mutant HTT protein induced disease-symptoms and pathogenic protein aggregation in mice [23]. In addition, Zhang et al. [22] found that human HEK293 T cells overexpressing mutant HTT-GFP fusion constructs release sEVs containing mutant HTT protein and its encoding RNA. Moreover, neural striatal cells were able to take up these sEVs and showed an increase in mutant *HTT* RNA. Thus, sEVs are able to deliver mutant *HTT* RNA from one cell to another [22].

All these studies show the potential of examining RNA organelles like stress granules and sEVs to gain insights into HD biology. RNA granules and sEVs share several characteristics: both originate from cytoplasm, are in the similar size range (100–200 nm), have a huge cargo of RNA

and proteins and there is an overlap of proteins present in RNA granules and sEVs. Many RNA-binding proteins that are a part of RNA granules help in loading sEVs during their formation. Moreover, liquid-liquid phase separation (LLPS), the process by which RNA granules form, helps in the sorting of biomolecules for sEVs as well [24–27]. To investigate a molecular connection between sEVs and RNA granules, we systematically analyzed the transcriptomic content of intracellular RNA granule cores and sEVs from an HD cell model and control cells. Our data show that intracellular RNA granules and extracellular RNA vesicles share content, several non-coding RNAs translocate to RNA granules, and the transcriptomic content of RNA granules and sEVs changes upon expression of mutant *HTT*.

2. Materials and methods

2.1. Cell culture

HEK293 cells stably expressing FLAG-tagged *HTT* exon 1 with 83 CAG repeats under an inducible Tet-off promoter [28] were cultivated in Dulbecco's Modified Eagle's Medium (DMEM) supplemented with 10 % tetracycline free FCS, 2 mM glutamine, 150 µg/mL hygromycin and 10 ng/mL doxycycline. To prepare the EV depleted media, tetracycline free FCS was centrifuged at 100,000×g for 20 h at 4°C. The supernatant was filtered with 0.22 µm filters and used for the preparation of culture media. 3×10^6 cells were seeded in 150 cm² culture dishes in EV depleted media. 8 dishes were treated with 10 ng/mL doxycycline to keep the cells uninduced (control), while the expression of *HTT* exon 1 was induced by washing off doxycycline in another 8 dishes (HD). The cells were incubated at 37°C and 8 % CO₂ for 72 h. After 72 h, the medium was collected, and the cells were treated with 0.5 mM sodium arsenite and incubated at 37°C at 8 % CO₂ for 55 min and then harvested using a cell scraper in 3 mL PBS. Finally, the cells were pooled, pelleted by centrifugation, and the pellet was stored in –80°C.

2.2. Isolation of sEVs and cytoplasmic RNA granule cores from HEK Q83 cells

sEVs were isolated from the culture medium by using the differential ultracentrifugation technique [29]. Briefly, low speed centrifugations at 300×g for 10 min and 2000×g for 20 min at 4°C were done to pellet cells, cell debris, and large vesicles like apoptotic bodies. The supernatant was then spun at 16,000×g for 30 min to remove larger vesicles like microvesicles [29,30]. Then the sEV were pelleted by centrifuging the supernatant at 100,000×g for 1 h 10 min at 4°C (AVANTI JXN-30, Beckmann Coulter). The pellets were resuspended in 2–3 mL PBS and recentrifuged at 100,000×g for 1 h 10 min at 4°C. Finally, the supernatant was removed, the sEVs were resuspended in 300 µL PBS and stored at –80°C until further use.

Cytoplasmic RNA granule cores were isolated by adapting the isolation procedure established by Namkoong et al. [31]. Briefly, the frozen cell pellets were thawed on ice and resuspended in 5 mL ice cold RNA granule lysis buffer (50 mM Tris pH 7.6, 50 mM NaCl, 5 mM MgCl₂, 0.1 % NP-40, 1 mM β-mercaptoethanol, 1x EDTA-free protease inhibitor cocktail, 0.4 U/mL RNase inhibitor). The cells were then lysed using a Dounce homogenizer (30 strokes per mL) and centrifuged at 2000×g for 2 min to remove the nuclear fraction and cell debris. The nuclear pellet was dissolved in nuclease-free water and analyzed as the nuclear fraction in the western blot experiments. The supernatant was collected (an aliquot of the supernatant was analyzed as the cytosolic fraction in the western blot experiments) and centrifuged at 10,000×g for 10 min to separate the soluble fraction of proteins from the insoluble RNA granule cores/pellet fraction. The resulting pellet was resuspended in 350 µL HPLC grade water and stored at –20°C until further use.

2.3. Characterization of the isolated sEVs and cytoplasmic RNA granule cores

The characterization of sEVs was done according to the MISEV guidelines 2018 and 2023 [14,32]. sEVs were characterized by detecting various positive and negative markers by western blot analysis, the vesicular size and particle number were determined using nanoparticle tracking analysis (NTA) and the morphology was analyzed by scanning electron microscopy (SEM). Cytoplasmic RNA granule cores were characterized by western blot.

2.3.1. Nanoparticle tracking analysis (NTA)

NTA was done using the ZetaView® particle analyser. Briefly, sEV-samples were diluted in the ratio of 1:1000 with sterile PBS. The sample sensitivity was set to 80.00 and the and shutter to 120. The sample chamber was flooded with PBS until no particles were seen. 1 mL sample was loaded with a syringe and the particle drift was checked. The samples were then measured at 11 positions in 3 cycles and the size distribution was obtained.

2.3.2. Scanning electron microscopy (SEM)

For size and morphological characterization of the sEVs, SEM (FEI DualBeam Helios NanoLab 600 (FIB)) was used. The sEV samples were thawed and dialysed to remove salts and other impurities (Slide-A-Lyzer™ MINI Dialysis Device, 2K MWCO, 0.1 mL). Silicon chips were cleaned by sequential sonication in acetone, ethanol and distilled water for 5 min each and were blow dried in a nitrogen stream. The sEV samples were diluted 1:1000 in sterile water and 0.5 µl of samples were spread on the cleaned silicon chips. The coated samples were then allowed to dry under the sterile hood for 10–15 min. To make the surface conductive, they were sputter coated with a gold layer of 5 nm thickness (SCD 050 Sputter Coater, BAL-TEC) before imaging by scanning electron microscope. Samples on silicon chips were mounted on a SEM stage by carbon paste and both close-up and wide-field images were taken at 10 KV.

2.3.3. Western blotting

For sEVs, equal volumes of RIPA buffer (50 mM TRIS HCL pH: 7.4, 150 mM NaCl, 1 % Triton X-100, 0.5 % sodium deoxycholate, 0.1 % SDS, 1 mM EDTA, protease inhibitor (cOmplete™ ULTRA) were added to the samples followed by an incubation for 30 min at 4°C. The samples were sonicated at 30 % intensity for 20 s. Cytoplasmic RNA granule cores were treated with benzonase for 30 min before addition of RIPA buffer. The samples were boiled with 2X Laemmli buffer, separated on an SDS-PAGE gel and transferred on a nitrocellulose membrane. The membranes were blocked with 5 % BSA and incubated with primary and secondary antibodies before detection on an iBRIGHT imaging system (Invitrogen).

Antibodies used: Anti-AIP/Alix antibody (BD biosciences) at 1:500 dilution, anti-Calnexin antibody (Abcam) at 1:1000 dilution, anti-HSP70 antibody (Enzo) in 1:1000 dilution, anti-Flotillin antibody (Abcam) in 1:1000 dilution, anti-eIF4E antibody (Cell Signalling Technology) in 1:1000 dilution, anti-FMRP antibody (Cell Signalling Technology) in 1:1000 dilution, anti-G3BP1 antibody (Santa Cruz) in 1:100 dilution, anti-YB1 antibody (Abcam) in 1:1000 dilution, anti-GAPDH antibody (Santa Cruz) in 1:1000 dilution, anti-Lamin A/C antibody (Santa Cruz) in 1:1000 dilution, mouse anti-rabbit IgG-HRP conjugated secondary antibody (Santa Cruz) in 1:1000 dilution, anti-mouse IgG HRP-linked secondary antibody (Cell Signalling Technology) in 1:1000 dilution.

2.4. RNA isolation

For the isolation of total RNA from sEVs and cytoplasmic RNA granule cores, mirVana™ miRNA Isolation Kit (Invitrogen) was used according to the manufacturers protocol.

2.5. RNA sequencing and quality control

For sEVs and RNA granules, five biological replicates were performed for each induced (HD) and non-induced conditions (control), yielding a total of 20 samples for RNA sequencing. For the preparation of whole-transcriptome sequencing-ready samples the Illumina stranded total RNA library preparation kit was used. Sequencing was performed on the Illumina NovaSeq platform, using S1 flow cells and 2x100 bp paired-end reads. One HD sEV sample only produced reads in thousands and was excluded from further analysis. On average, sEV samples yielded 14.4 million reads and RNA granule samples 45.3 million reads. FastQC (Version v0.12.1) was used to assess read quality (<http://www.bioinformatics.babraham.ac.uk/projects/fastq>). Quality trimming and filtering was performed in two steps. First, Trimmomatic [33] was used to remove adapter sequences and remove bases of quality below 20 from both ends of reads. Second, cutadapt [34] was used to cut the first three bases from reads, correct for high-quality, but incorrect “G” calls at the reads’ 3’ end (option `-nextseq-trim = 20`), additionally clipping repeats of ten “G”s and following sequences from read ends, and to trim poly-A and poly-T ends (option `-poly-a`). Read pairs in which one read was shorter than ten bp were discarded. On average, 85.8 % of read pairs passed quality filtering for the sEV samples, and 99.3 % for the RNA granule samples. Unpaired reads after quality filtering were discarded.

2.6. Quantitative RT-PCR (qRT-PCR)

Total RNA was isolated using the NEB Monarch kit (New England Biolabs). cDNA synthesis was done using the TaqMan reverse transcription reagents kit (Applied Biosystems), according to the manufacturer’s instructions and the following temperature profile was used: 25 °C for 10 min, 48 °C for 1 h, 95 °C for 5 min, and cooling down to 4 °C. Finally, quantitative real-time PCR was carried out using the SYBRGreen PCR master mix (qPCR BIO SyGreen Mix, Nippon). Samples were analyzed in triplicates.

Primers used (5’-3’): **HSALNT0279541 (LHR1-LNC1610-1)**: Forward primer (FP): CGTGAAGTCCGTGGAAGCCT, Reverse Primer (RP): CCCTCACCATTTCGACGG; **SNHG78**: FP: AGCTTCGGGAAGCCTGGA, RP: TTGAGGAGTACCCTGTTC; **HSALNT0088996 (lnc-SLC30A5-6)**: FP: AGTGAGAGACTGTGGCAGC, RP: GGCTGTCCATCTGTCTCCA; **HSALNT0398958 (lnc-DUXA-1)**: FP: TACTGGGCTGAGCTGGCATG, RP: TTGGCCTGTAGTGTGGGGTG; **SNHG12**: FP: ACAGAGATCCCGGC GTACTT, RP: GGCAATTCAGATCCCGGGC; **AGADH**: FP: ATG-GAAATCCCATCACCATCTT, RP: CGCCCACTTGATTTGG; **RPL22**: FP: TGACATCCGAGGTGCCTTTC, RP: GTTAGCAACTACGCGCAACC.

2.7. RNA-FISH

25,000 cells per well were seeded in poly lysine coated 8 chamber slides. The cells were then incubated for 72 h at 37°C and 8 % CO₂. For studying stress-response cells were treated with 0.5 mM arsenite solution for 55 min. After 55 min, the medium was removed, and RNA-FISH was done using the ViewRNA™ Cell Plus Assay Kit (Invitrogen). The assay was done according to the manufacturer’s protocol by using 3 probes: LHR1-LNC1610-1 (Alexa flour 546), SNHG7 (Alexa flour 488), lnc-DUXA-1 (Alexa flour 647) (Invitrogen™ ViewRNA™). A no probe control and a GAPDH probe were used as controls for the experiment. The detection of RNAs and the RNA granule protein marker YB1 was done by Zeiss LSM 900 (Airyscan 2) (Zeiss). Regions of interest (ROIs) (n = 6) were chosen around YB1-positive granules and colocalization analysis was done by using the BIOP JACoP image analysis plugin in the Fiji ImageJ software. To quantify the colocalization of transcripts in YB1-positive granules, Pearson’s (ranges between -1 and +1, 1 = perfectly, linearly related, -1 = perfectly, but inversely, related) and Spearman’s (ranges between -1 and +1, 1 = perfectly, linearly related, -1 = perfectly, but inversely, related) coefficients were retrieved.

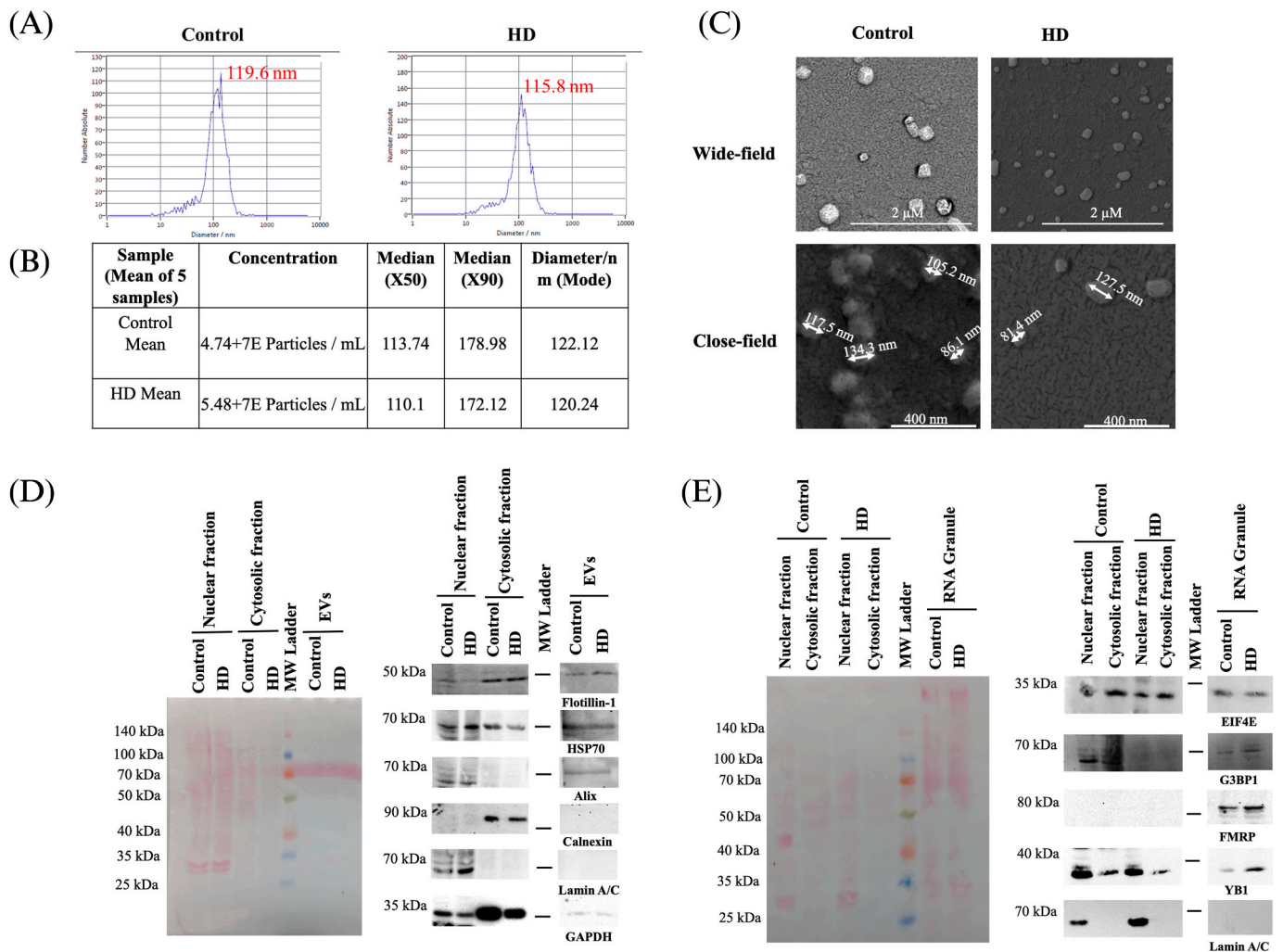


Fig. 1. Validation of successful sEV and RNA granule isolation: (A) Representative images of an NTA analysis of one control and one HD sEVs sample. The peak analysis shows that the size range of particles that were most recurrently measured is 119.6 nm and 115.8 nm, respectively. (B) The table contains mean values from the NTA analysis of all five replicates of sEVs. The term median X90 represents the diameter of the particles where 90 % of the distribution has smaller and 10 % has larger particle size than the given diameter. (C) Wide-field and close-field SEM images of control and HD sEVs. SEM images show round-shaped morphology of sEVs with the expected size range between 50 and 200 nm confirming the presence of sEVs. (D) Western blots of sEV samples. The presence of sEV markers AIP1/ALIX, Hsp70, Flotillin and absence of contaminant markers Lamin A/C and Calnexin confirm the presence of sEVs in the samples (right panel). The total protein load was visualized by Ponceau staining (left panel). (E) Western blots of RNA granule samples. The successful isolation of cytoplasmic RNA granule cores is shown by the presence of EIF4E (SG marker), G3BP1 (SG marker), FMRP (SG/p-body marker) and YB1 (SG/p-body marker) and the absence of Lamin A/C (right panel). The total protein load was visualized by Ponceau staining (left panel).

2.8. Data analysis

2.8.1. Transcript mapping and quantification

For read alignment and quantification, Salmon [35] (Version 1.10.2) was used in mapping-based mode, following the pseudoalignment strategy. The reference database was constructed by non-redundantly combining GENCODE transcript sequences (Release 44, GRCh38.p14) with sequences from RNACentral (Release 22) annotated as “*Homo sapiens* (human)”, resulting in 921,552 unique sequences. The index was constructed using a *k*-mer length of 13 (option “-k 13”) and using the entire genome as decoy sequence. Mapping and quantification of sample reads were then performed choosing IU as the library type and using the options “-numBootstraps 100 -seqBias -gcBias”. The average mapping rate over all samples was 72.3 %. Salmon transcript output was then processed using tximport (Version 1.26.1), in R [36] and collapsed to the gene level. Note that by this approach, non-coding RNA transcripts from the RNACentral database (incorrectly) appear as ‘genes’ in downstream analysis. Hence, when referring to ‘genes’, this always also includes non-coding RNAs from here on. To identify genes, which were specific

for a condition, we only considered genes that were consistently detected within at least one of the four conditions tested (sEVs/RNA granules, induced (HD) and non-induced (control), termed “consistent genes”). Such genes had to have an abundance ≥ 10 counts in all samples belonging to the respective condition, allowing for one mismatch.

For comparing our cell line results with patient data, we obtained raw sequencing data from a RNA sequencing study focusing on plasma extracellular vesicles [37]. The data set comprised 59 samples grouped into four patient classes (21 healthy individuals - ‘control’, 19 HD individuals without clinical signs - ‘pre-HD’, and 19 HD patients with early clinical signs - ‘early-HD’). Sequencing data was processed as described above, except for trimming ten “T”s at the 5’ end of reverse reads instead of 3 bps, and clipping ten “A”s and following sequences from read ends. On average, 11.2 million reads were available per sample, of which 99.9 % passed quality control, and the average mapping rate was 9.3 %. All data analysis was performed in R (Versions 4.2.2 and 4.1.2, <https://www.r-project.org/>).

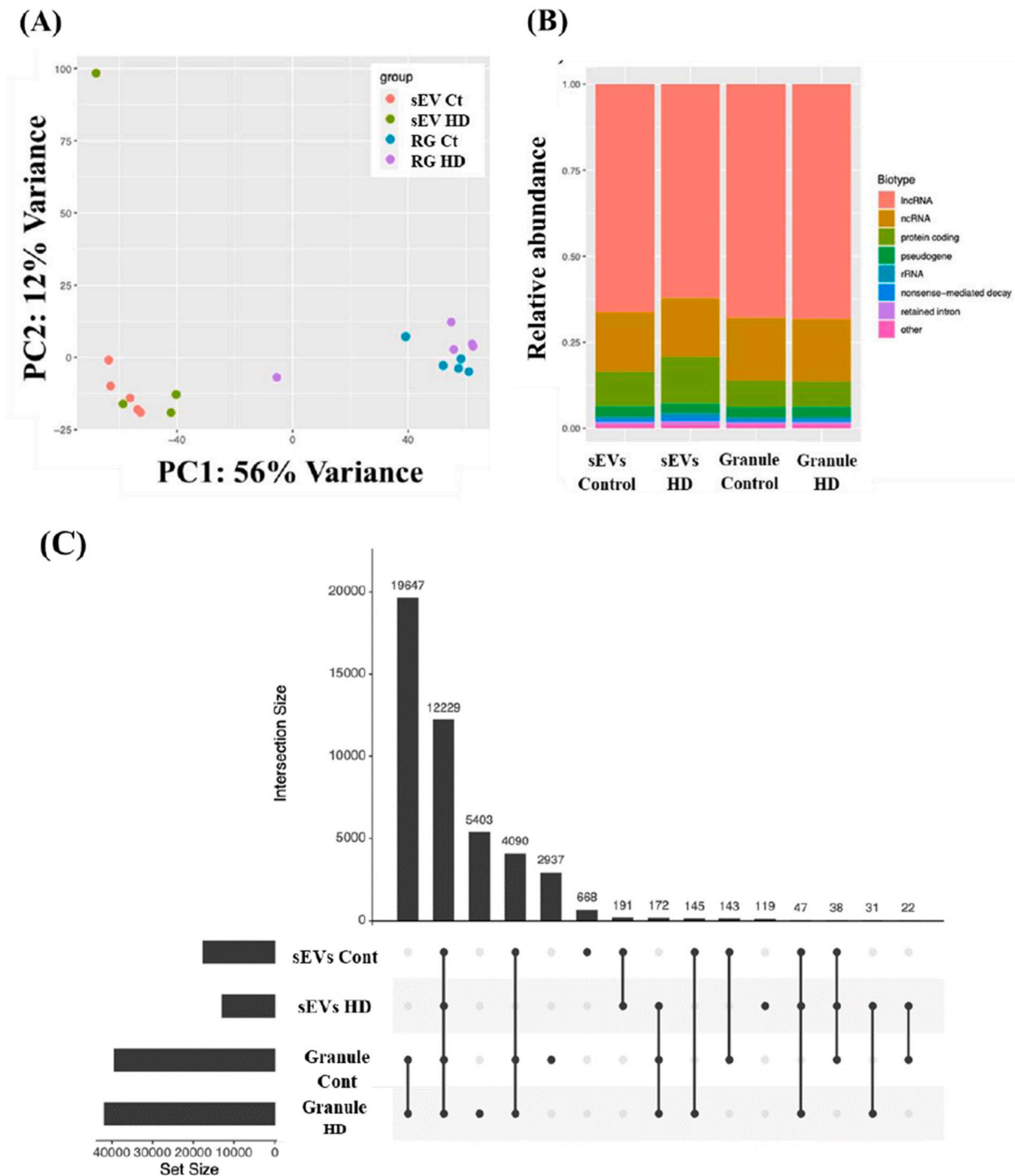


Fig. 2. Composition of detected RNAs in the different conditions: (A) Principal Component Analysis (PCA) plot of gene content in sEV and RNA granule samples from control and HD cells to assess similarity in gene composition across samples. (B) Relative composition of the detected RNAs. (C) Distribution of 45,882 consistently detected genes across all four combinations of sample type (sEV and RNA granules) and condition (control and HD). 12,229 genes were present in all four combinations (second vertical bar with vertical line below connecting four dots), while fewer genes were unique to each combination (vertical bars with single dot below). Granule samples contained more consistently detected genes than exosome samples (horizontal bars).

2.8.2. Differential analysis

We performed two separate analyses to characterize the difference in gene content across sEV and RNA granule samples under control and HD conditions. The first analysis was based on the presence or absence of genes from the respective condition. We focused on genes which were consistently detected under HD conditions (i.e., genes had an abundance ≥ 10 counts in all HD samples, only allowing for one exception), but not under control conditions (i.e., zero counts in all control conditions as the

strictest choice), or vice versa for both sEV and RNA granule samples. This procedure delivers genes that are most discriminative for HD and control conditions as best candidates for marker genes.

In the second analysis, gene abundance was additionally taken into account by performing a differential gene expression analysis using DESeq2 [38] to elucidate changes between control and HD conditions for sEV and RNA granule samples. All genes were included in analysis that had an abundance of ≥ 10 counts in at least one sample. An adjusted

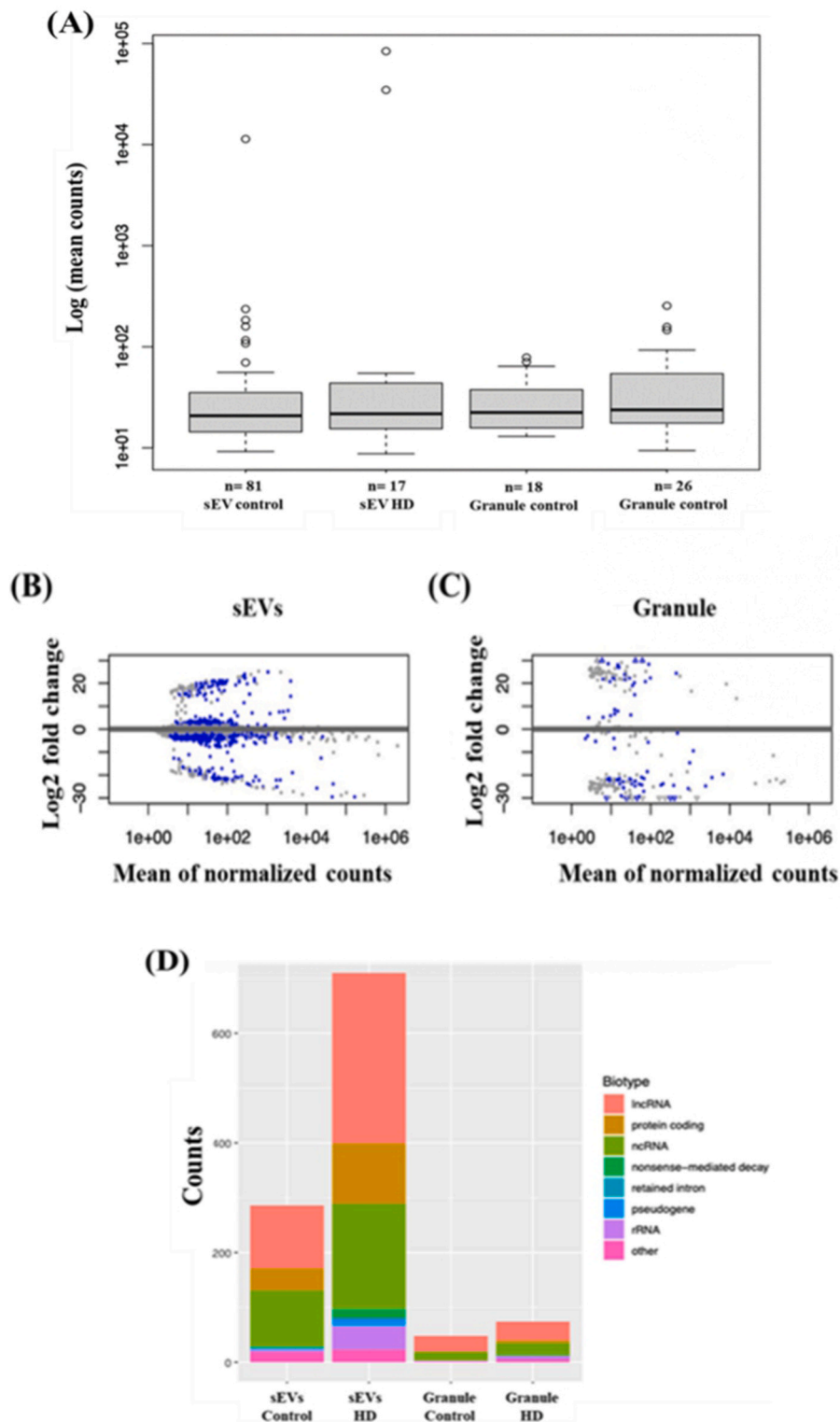


Fig. 3. Differentially expressed genes: (A) Mean count abundance of marker gene candidates that were consistently present in samples of one condition (x-axis), but fully absent in the opposing condition (i.e., HD for control samples and vice versa). (B,C) Differential gene expression analysis comparing HD and control conditions: Negative fold changes indicate an increase in HD cells, positive fold changes indicate and decrease in HD cells. To improve the visualization by reducing noise due to low count genes, fold-changes were reduced using an adaptive shrinkage estimator before plotting. (B) For sEV samples, 707 genes were enriched and 241 were depleted after HD-induction. (C) For RNA granule samples, 53 genes were enriched, and 33 were depleted (adjusted p-value 0.05). (D) Biotype of marker transcripts indicative for respective sample type and condition.

p-value of 0.05 was chosen and log-fold changes were reduced for visualization by applying the adaptive shrinkage estimator *ashr* [39]. We finally merged the differentially expressed genes as obtained by both approaches in a unified list of marker genes for the specific conditions (see supplementary file, sheet 'Marker genes').

2.9. STRING and GO term enrichment analysis

STRING V12.0 was used for performing functional analysis of marker gene candidates [40]. On the search mode, the multiple proteins option was selected and the query gene names (marker genes (HD sEVs and RNA granules, and control sEV and RNA granules as two different queries)) were uploaded. The analysis was done in the *Homo sapiens* mode and the interaction score of 0.7 (high confidence rate) was chosen. Weak interaction sources like text mining and neighbourhood were omitted during the analysis. GO term enrichment analysis was done using the Gene Ontology knowledgebase. Panther overrepresentation test was done (PANTHER 18.0). Fischer exact test was chosen and false discovery rate was calculated [41–43].

3. Results

3.1. Isolation and characterization of sEVs and RNA granules

To perform a comparative analysis of the RNA content of intracellular RNA granules and sEVs in response to expression of mutant *HTT*, we made use of an inducible HD cell model, which expresses FLAG-tagged *HTT* exon 1 with 83 CAG repeats under an inducible Tet-off promoter. The benefit of using this cell model is that it represents a robust human cell system with high expression of mutant *HTT* exon1, meaning a severe phenotype that will give rise to fast results. Any differences detected in this monoclonal cell model are clearly caused by expression of mutant *HTT* and effects of other factors (e.g., environmental factors or genetic variants) affecting composition of RNA granules and sEVs can be excluded.

sEVs and cytoplasmic RNA granule cores were isolated from both induced (HD) and non-induced (control) cells. To validate successful isolation, different techniques were used. The characterization of sEVs was done using three different readout techniques: (I) We performed NTA analysis on 5 biological replicates. The average amount of particles in control and HD samples were 4,74E+07 particles/ml (1:1000 dilution) and 5.48E+07 particles/ml (1:1000 dilution), respectively. The mean diameters of control and HD sEVs were 122.12 nm and 120.24 nm, respectively. Thus, these analyses confirmed the expected average particle size (between 50 and 200 nm) (Fig. 1A and B). (II) SEM images showed the round-shaped morphology of sEVs with the expected size range between 50 and 200 nm (Fig. 1C). (III) The presence of sEV markers AIP1/ALIX, Hsp70, Flotillin and absence of the contaminant markers like Lamin A/C and Calnexin were shown by western blot (Fig. 1D). The successful isolation of cytoplasmic RNA granules cores was confirmed by detecting EIF4E (SG marker), G3BP1 (SG marker), FMRP (SG/p-body marker) and YB1 (SG/p-body marker) on western blot (Fig. 1E). The nuclear and cytoplasmic fractions represent the pellet and supernatant from the first centrifugation during the RNA granule or sEV isolation, respectively.

3.2. Analysis of RNA content of sEVs and RNA granules

From the successfully isolated sEVs and cytoplasmic RNA granule cores, RNA was isolated and subjected to RNA sequencing to analyze their RNA content. Out of a total of 303,919 detected genes in all samples, 95,856 genes had an abundance of ≥ 10 counts in at least one sample (31,5 %). sEV and RNA granule samples were clearly separated regarding gene content (Fig. 2A). However, no clear separation of control and HD samples was visible. One outlier was detected for sEV HD samples. As this condition already contained one sample less than the

other conditions, we decided to keep this outlier in the analysis. Instead, we allowed for one absence in samples and still considered the gene to be consistently detected in the respective condition (see Methods). The RNA composition only slightly varied between conditions (Fig. 2B). The top three fractions were long non-coding RNAs (making up between 62- and 68 % of total RNAs), non-coding genes (17–18 %), and protein coding genes (7–10 %, Fig. 2, Supplementary File 1). Only in granule samples, a minor fraction of miRNAs was detected with a total of 25 under control conditions (0,012 %) and 23 under HD conditions (0,010 %).

A total of 45,882 genes were consistently detected across samples belonging to at least one condition and subjected to further analysis. RNA granule samples featured a higher count in these genes with a median of 44,048 genes under control conditions and 44,319 under HD conditions than sEV samples with 34,439 under control conditions and 26,100 under HD conditions (Supplementary Fig. S1A). The composition of consistent genes was identical among conditions. In comparison to all detected genes, as reported above, the share of long non-coding RNAs was lower (46–49 %) and higher for protein coding genes (26–28 %), and the share of non-coding genes remained similar (16–18 %, Fig. S1B). The difference in gene composition between sEV and RNA granule samples also became apparent when comparing unique and shared consistent genes between all conditions (Fig. 2C). A large fraction with 27,987 genes (61.0 %) was unique to RNA granule samples. Another large fraction with 12,229 genes (26.7 %) was consistently present under all conditions. When comparing control with HD conditions, the majority of genes were common to both conditions and only small fractions were exclusive for either condition. For the sEV samples, 12,505 genes (27.3 %) were common to both conditions and only 5046 genes (11.0 %) were exclusive for control, and 344 genes (0,7 %) for HD conditions. This was even more extreme for the granule samples with 36,138 genes (78,8 %) common to both conditions and only 3140 genes (6,8 %) exclusive for control, and 5626 genes (12,3 %) for HD conditions.

3.3. Differentially enriched genes

To identify genes, which were differentially enriched under control and HD conditions, we applied two approaches: while only presence or absence of genes was considered in the first approach, gene abundances were additionally considered in the second approach. For the first approach, we examined consistent genes and selected those, which were present in either condition but completely absent in any sample of the opposing condition. We found between 17 and 81 of such genes across the conditions, with varying mean count abundances in the respective marked condition (Fig. 3A, Supplementary File 1). For the second approach to consider the abundance of genes in the analysis, we performed a differential gene expression analysis using DESeq2. Out of 95,856 tested genes, 948 were found to be differentially abundant in control and HD conditions for sEV samples (707 enriched and 241 depleted under HD conditions), and 86 for RNA granule samples (53 enriched and 33 depleted, Fig. 3B and C). By combining the differentially regulated genes identified by both approaches, we obtained a list of 1091 genes, which were enriched or depleted under HD conditions for sEVs and/or RNA granules (Supplementary File 1). A total of 58 genes were detected by both approaches, while 84 genes were exclusively identified by the presence/absence approach, and 949 genes were exclusively detected by DESeq2 analysis. Overall, more genes were indicative for HD conditions (i.e., they were enriched under HD conditions with 710 genes for sEVs and 74 genes for RNA granules) than for control conditions (286 genes for sEVs and 48 genes for RNA granules). Long non-coding and non-coding RNAs were the major contributors to these marker genes, with the sEV samples additionally featuring a sizable fraction of protein coding RNAs (Fig. 3D). A considerable fraction of the inferred marker gene list was found to be under regulatory control by the transcriptional repressor RE1 silencing transcription

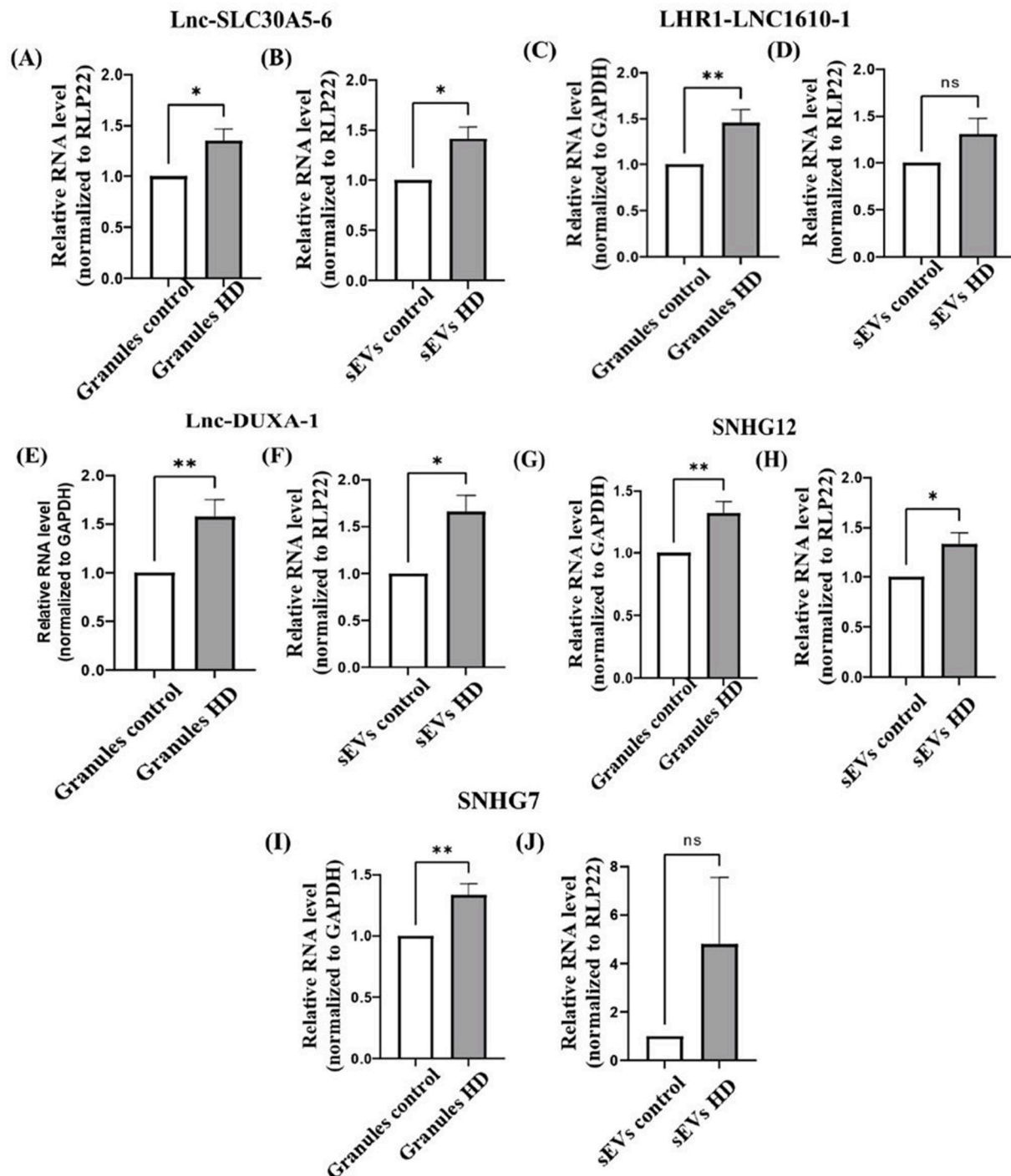


Fig. 4. Validation of increased RNA levels in HD RNA granules and sEVs: To validate the RNAseq results, the relative RNA level of the marker genes Lnc-SLC30A5-6 (A,B) ($n_{sEVs} = 3$; $n_{RNA\ granules} = 3$), LHR1-LNC1610-1 (C, D) ($n_{sEVs} = 5$; $n_{RNA\ granules} = 10$), Lnc-DUXA-1 (E, F; $n_{sEVs} = 3$; $n_{RNA\ granules} = 8$), SNHG12 (G, H) ($n_{sEVs} = 4$; $n_{RNA\ granules} = 15$), and SNHG7 (I, J) ($n_{sEVs} = 4$; $n_{RNA\ granules} = 10$) in RNA granule and sEVs fractions from HD cells and controls was measured by qRT-PCR. The relative expression level of the marker genes, normalized to a housekeeping gene (RPL22 or GAPDH), is shown in RNA granules (A, C, E, G, I) and sEVs (B, D, F, H, J). Columns indicate mean values \pm SEM. * $p < 0,05$.

factor (REST) according to the TFLink database [44] (139 genes, [Supplementary File 1](#)). When comparing sEVs with RNA granules, we identified six genes which were indicative for HD condition for both sample types, and five genes which were consistently indicative for control conditions ([Supplementary File 1](#)). We confirmed the increased abundance of five HD marker genes in RNA granules and sEVs by another readout technique, namely qRT-PCR. For RNA granules we could confirm an increase in HD samples for all five marker genes. For

sEVs, while we detected an increase in every single experiment, two out of the five transcripts failed a statistically significant effect due to high variability between the replicates ([Fig. 4](#)). To validate the co-localization of the top three selected transcripts based on the mean abundance values (LHR1-LNC1610-1, SNHG7 and Lnc-DUXA-1) with RNA granule markers, RNA-FISH was done. As controls for successful staining GAPDH and a no probe control were analyzed at the same parameters ([Supplementary Figs. S2, S3, S4 and S5](#)). We found a partial

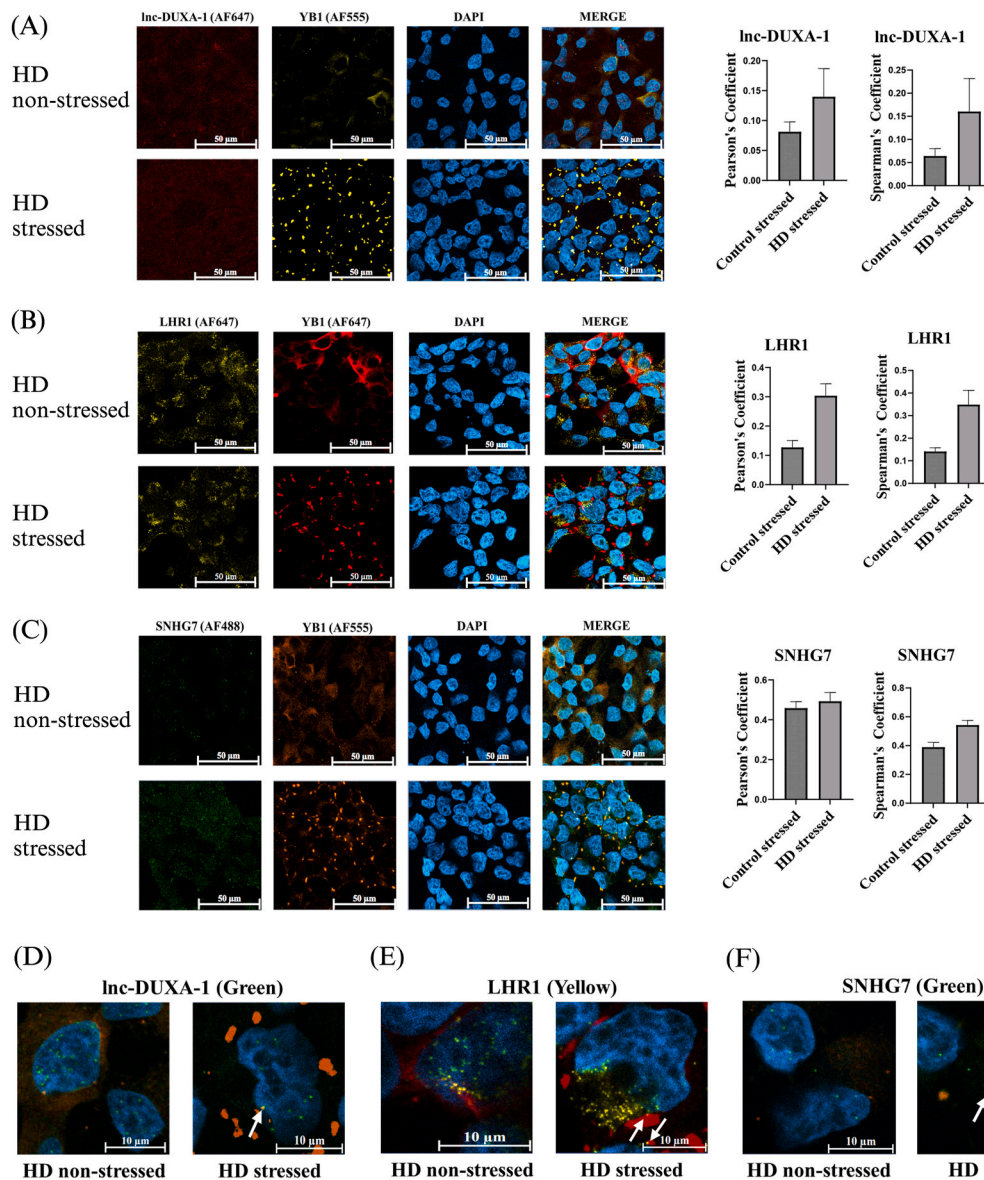


Fig. 5. RNA-FISH analysis: Images of non-stressed cells and stressed HD cells stained with YB1 antibodies (YB1-positive RNA granules) and probes detecting the three HD marker transcripts DUXA1 (A), LHR1 (B) and SNHG7 (C). **Right panel:** Colocalization analysis of control and HD stressed cells. The graphs show comparative analysis of the mean values of Pearson's coefficients and Spearman's coefficients. (D, E, F) Representative cells from the images shown in (A, B, C) are also shown at a higher magnification. The white arrows indicate sites of colocalization of transcripts DUXA1, LHR1 and SNHG7 with YB1-positive RNA granules.

colocalization of our marker RNA transcripts in YB1-positive RNA granules (Fig. 5). This is in line with the fact that stress-induced granules show variability in their composition [26]. For quantifying the colocalization, different coefficients of correlation were obtained and compared in control and HD stressed cells (due to the presence of YB1-positive granules). All the 3 transcripts showed higher coefficients of correlation in the HD stressed cells when compared to control stressed cells (Fig. 5, Supplementary File 2). However, for the transcript SNHG7, the coefficients only showed a slight increase, which may be explained by relatively high background. Taken together, the colocalization studies not only confirmed the colocalization of the transcripts with an RNA granule marker, but also showed a substantial increase in the colocalization of transcripts in HD conditions.

3.4. Comparison with patient data

To investigate, if the above-mentioned enriched and depleted genes that we detected in our monoclonal cell line model are also detectable in

patient samples, we compared our data to a recently published dataset of HD patient samples [37]. The analysis of the RNA sequencing data set obtained from plasma EVs from patients contrasting the three conditions "control", "pre-HD", and "early-HD" revealed a total of 330,551 genes over all samples, of which 21,848 genes (6.6%) had an abundance of ≥ 10 counts in at least one sample. We used these data to derive fold changes by DESeq2 and to compare the direction of change of our HD marker genes between our cell line data and patient data.

To focus on a robust signal in patient data, we only considered genes that featured a log2 fold change beyond ± 0.5 . For our marker genes for sEVs, 66 patient genes were available for comparison when contrasting "control" vs. "pre-HD" conditions (Fig. 6). Of these, the fold change direction agreed for 34 genes (51.5%). For the comparison "control" vs. "early-HD", 73 genes were available for comparison of which 28 agreed (38.4%). Thus, a better agreement was consistently achieved for the "pre-HD" condition, indicating that our system might be more comparable to a state of very early HD onset.

To check whether any of our marker genes have been previously

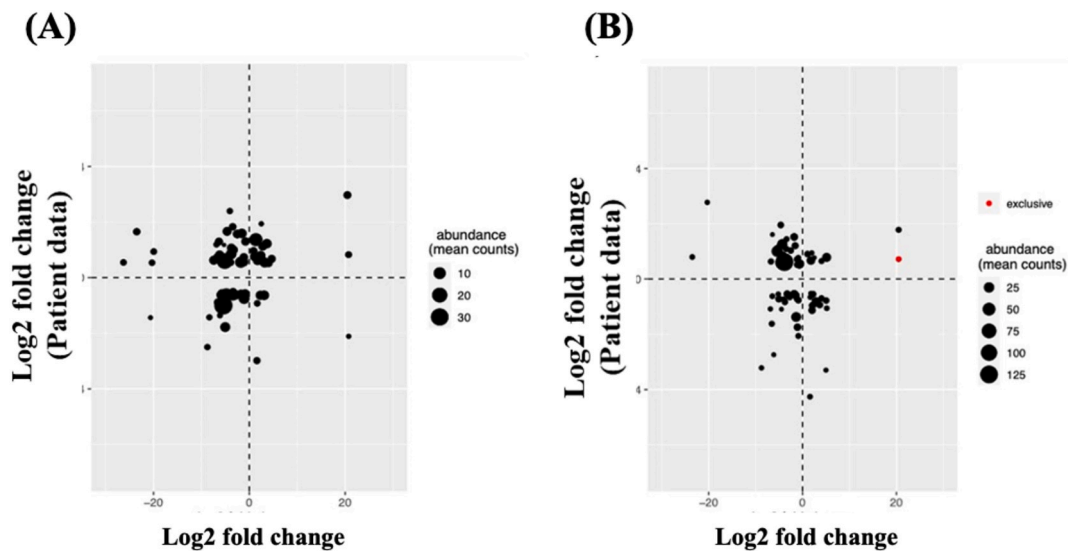


Fig. 6. Comparing log₂ fold changes of marker genes: comparison of “control” vs. “pre-HD” (A), and “control” vs. “early-HD” (B). x-axis: Log₂ fold change in patient data; y-axis: Log₂ fold change in data from HD cell line model sEVs. Symbol size indicates mean count abundance in patient data. Only genes with a log₂ fold change beyond ± 0.5 in patient data were considered. Genes marked “exclusive” were absent in the opposing condition, hence no fold change was available and the maximal occurring fold change value was used instead for the x-coordinate.

linked to HD, we compared the list of our marker genes with a published list of the top 20 differentially expressed genes in HD across ten categories [45]. We found two matches: We found the gene *PLCB1* to be enriched under HD conditions in sEVs (log₂FC 0.8), which also has been reported as one of the top 20 differentially expressed genes in the category “Pluripotent”, although having been reported as being down-regulated in HD (log₂FC -1.0 , [46]). Gene *CDH10* (category Brain_late_striatal_neuronal_interneuron) is the second match of list of the top 20 differentially expressed genes in HD. We found it down-regulated under HD conditions for sEVs in our dataset (log₂FC -3.7).

3.5. STRING and GO term enrichment analysis of the marker genes

The derived marker gene sets being indicative for control or HD conditions were subjected to STRING and GO term enrichment analysis to elucidate common functional features and any known or predicted interactions. While no significant enrichment was detected and no interactions were found at the interaction score of 0.7 (high confidence) in the control (RNA granule and sEV marker genes) dataset as well as in the HD RNA granule data, STRING analysis of HD marker genes from HD sEVs showed significantly more interactions than expected with a PPI enrichment value of 0.000539 at the interaction score of 0.7 (high confidence). GO term enrichment analysis of HD marker proteins from sEV also showed hits for terms related to EVs (Fig. 7). Of note, only approximately one third of our detected RNA transcripts have an Ensembl ID and thus could not be included into the STRING and GO term enrichment analysis.

4. Discussion

RNA organelles such as RNA granules and sEVs are an integral part of the cell’s regulatory network. Cells under stress respond by RNA granule formation, and increased sEV secretion. sEVs and RNA granules meet on several common grounds such as their site of origin, cargo, and the involvement of LLPS. There is increasing evidence that an overlap of content between SGs, p-bodies and sEVs exists. Several studies individually investigated sEVs and RNA granules in different neurodegenerative conditions including HD [12,13,23,47,48]. However, their shared transcriptomic cargo remains poorly explored. To establish a link

between these organelles and investigate the crosstalk between them, we isolated sEVs and RNA granules from an HD cell model and analyzed their transcriptome. Our transcriptomic analysis revealed that the largest chunk of RNAs in both sEVs and RNA granules were ncRNAs. ncRNAs offer extensive opportunities for early diagnosis and therapeutic interventions in several neurodegenerative disorders [49]. ncRNAs include miRNAs that are involved in the manifestation and progression of several diseases. Several recent studies suggest that neural-derived sEVs and their miRNA cargo give rise to disease-specific signatures in neurodegeneration [50,51]. However, in our dataset, we failed to detect miRNAs in sEVs and only detected a minor fraction of miRNAs in RNA granule samples. The failure to detect miRNAs in sEVs might be related to lower read abundance (approx. factor 3) and lower read quality (13.5 percentage point reduction in reads passing initial quality filtering) achieved for sEV samples in comparison to RNA granule samples. A reason for this may be that we did not use a protocol that enriches for small RNAs in our RNA sequencing procedure.

In contrast, in our dataset, lncRNAs had the highest abundance rates in both control and HD datasets. lncRNAs are a class of ncRNAs that are highly conserved and longer than 200 nucleotides. lncRNAs can form complex secondary structures leading to the formation of sites that allow intermolecular interactions. These interactions aid several biological functions involving growth, development, cell proliferation, differentiation and apoptosis [52–54]. lncRNAs interact with biomolecules such as proteins and miRNA and modulate their target’s expression at genetic, transcriptional and post-transcriptional levels [55]. Since lncRNAs are involved in a plethora of biological processes, aberrant regulation of lncRNAs contributes to the pathogenesis various neurodegenerative disorders including HD. Several studies have validated the contribution of lncRNAs in the progression of HD: The nuclear translocation of the REST transcription factor is regulated by wild-type HTT. Mutations in the *HTT* gene lead to abnormal nuclear-cytoplasmic transport of REST resulting in aberrant expression of REST target genes [56–58]. The expression of the lncRNA Human Accelerated Region 1 (*HAR1*) is decreased in the striatum of HD patients. The reason for this is an increased cytoplasmic translocation of REST leading to the inhibition of *HAR1* transcription [59]. Along with *HAR1*, the expression levels of several other lncRNAs like *NEAT1* and *MEG3* is hindered due to aberrant REST translocation [60–62]. Moreover, the lncRNA *NEAT1* that plays a neuroprotective role in HD was found to be overexpressed in HD patient

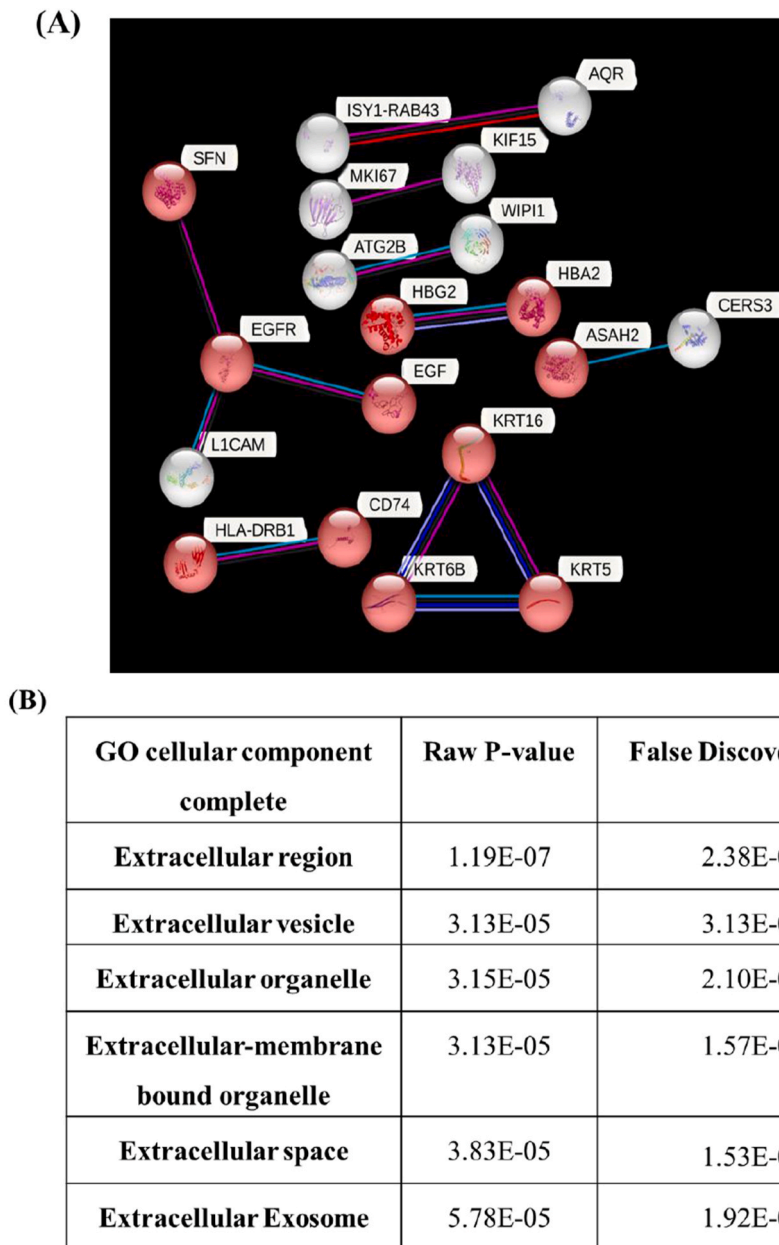


Fig. 7. STRING analysis of HD marker genes in sEV samples: (A) The red bubbles indicate the genes that were associated with extracellular region with a false discovery rate (FDR) of 0.00044. (B) GO term enrichment analysis of HD marker genes in sEV samples shows hits for terms related to EVs. The false discovery rate (FDR) indicates the number of false discoveries among the set of significant tests. Both the low P-values and FDRs indicate that the results are highly statistically significant.

brains and R6/2 mice [63]. Of these lncRNAs known to relate to HD, we found *NEAT1* in our dataset, but only in sEVs from control samples. *NEAT1* is upregulated in HD [63], meaning that its intercellular transcript level is increased. However, this may not be reflected in an increased transcript level in sEVs secreted from HD cells. We detected *NEAT1* only in sEVs secreted from control cells. While it is presumed that lncRNAs, which are abundant in cells, will also be abundant in sEVs, the scientific data reports otherwise. Studies have shown that there is a selective abundance of certain lncRNAs in sEVs compared to their mother cells, suggesting distinct lncRNA loading into EVs [64,65]. Thus, one could speculate that HD cells may retain *NEAT1* intracellularly due to its protective function and therefore do not secrete it. Moreover, a considerable fraction of our marker transcripts was found to be under regulatory control by REST according to the TFLink database [44], highlighting the importance of REST signaling in HD (Supplementary

File 1).

In our study, we identified RNAs that are present both in sEVs and RNA granules. Showing that intracellular RNA granules and extracellular sEVs share transcriptomic cargo indicates their presumed association. One explanation for this shared content may be that sEVs could enclose RNA granules to relieve cells from RNA granules in the diseased state. Further, we report a specific signature of transcripts in sEVs and RNA granules of HD samples. STRING and GO term enrichment analysis suggest a functional association between transcripts that get secreted from HD cells. Of note, one the major limitation of STRING and GO term enrichment analysis of our data is the fact that these tools lack genes from RNA Central. In our dataset, we had three times more genes from RNA Central than Ensembl. Thus, our downstream analysis using STRING and GO term enrichment analysis is limited.

Our study was conducted on a monoclonal HEK cell model. The

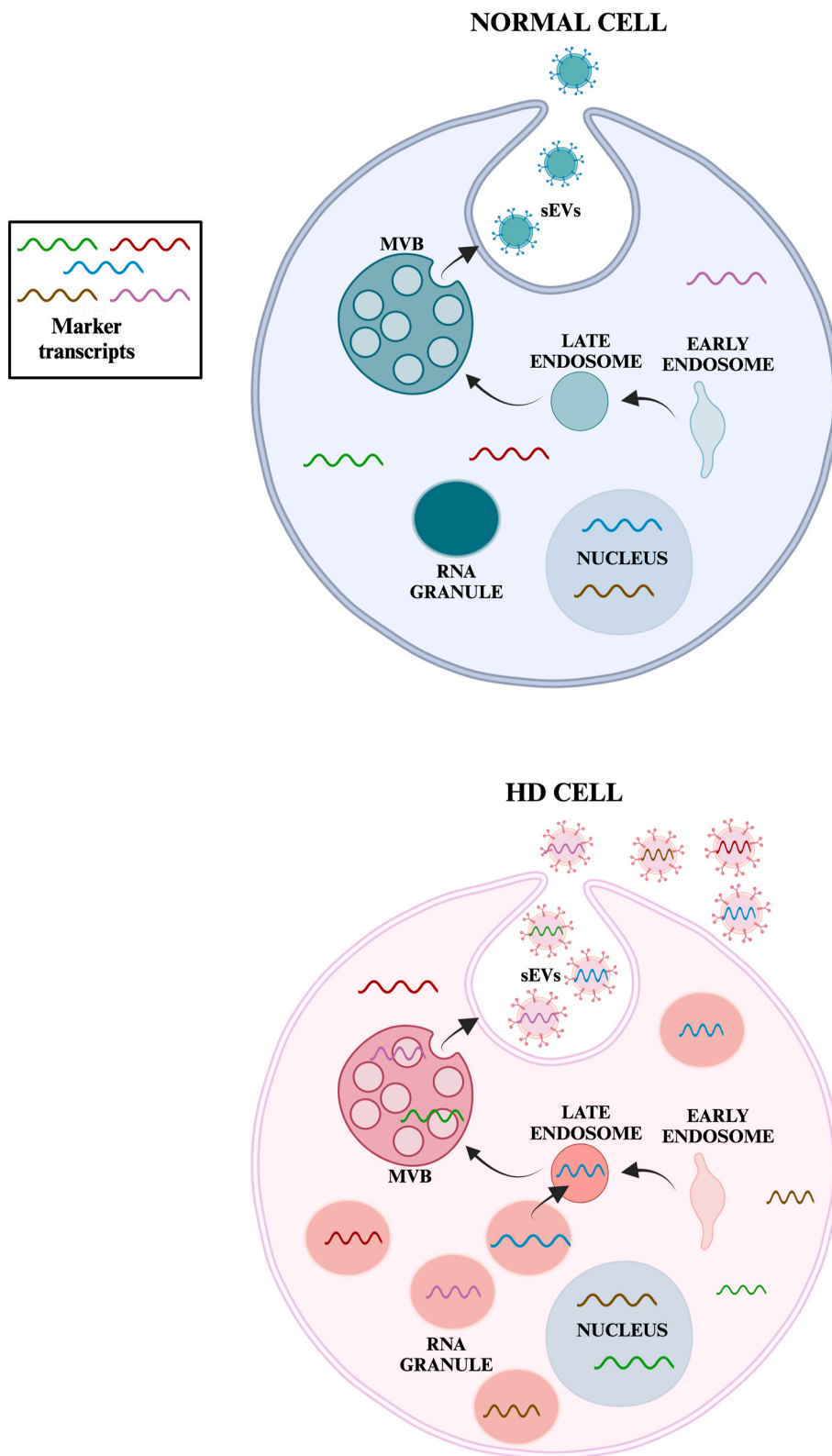


Fig. 8. Proposed model: CAG repeat mutations in the *HTT* gene affect the formation of cytoplasmic RNA granules and sEVs. Intracellular RNA granules and sEVs share content, suggesting that formation of RNA granules and sEV-loading may be related. sEVs originate from the early endosome and may take up RNA granule content during their maturation inside the multivesicular bodies (MVB). Upon expression of mutant *HTT*, SG formation and sEV secretion increase. In HD cells, specific marker transcripts (indicated as red, blue, green, brown, and purple structures) accumulate inside RNA granules and sEVs. Thus, the composition of RNA granules and sEVs changes upon expression of mutant *HTT*. Of note, both RNA granules and sEVs show a high variability in their transcript cargo. Created with [Biornder.com](https://www.biornder.com).

benefit of using such a cell model is that it represents a robust human cell system with high expression of mutant *HTT* exon1, meaning a severe phenotype that will give rise to fast results. Different to the analysis of patient and control samples (like blood or CSF), any differences detected in this monoclonal cell model are solely caused by expression of mutant *HTT*. This allows a mechanistic analysis of cellular pathways affected by expression mutant *HTT*. However, this cell model has its limitations: it is not a neuronal cell line and thus may not present brain cell-type specific expression differences in transcripts that are affected by expression of mutant *HTT*. Additionally, our model only expresses *HTT* exon1 and not the full-length transcript. However, several studies support that exon1 transcripts are a valuable model, since aberrant splicing of mutant *HTT* generates a small polyadenylated *HTT* exon1 mRNA that encodes the highly pathogenic polyglutamine protein in disease tissue [66–68]. Moreover, the situation in patients may be different since environmental factors or genetic variants may also affect the composition of EVs and RNA granules in patients. Thus, we compared our dataset to data from HD patient samples. The comparison of our data with a study of EVs isolated from patient biofluids like blood [37] revealed a 51,5 % percent overlap with genes differentially expressed in pre-HD samples. This overlap is bigger than the overlap with genes detected in symptomatic patients (38,4 %). This may be explained by the fact that our cell model represents an early phenotype, since the mutant *HTT* construct was expressed for a relatively short (72 h) interval prior analysis. The observation that we did not detect all the genes differentially expressed in pre-HD samples in our HD cell line model can be explained by the fact that other factors than solely the expression of mutant *HTT*, e.g., lifestyle or other genetic variants, may affect composition of EVs. *G3BP1*, which has previously been connected to HD [12,69] and was found greater than twofold upregulated in early-HD [37], was detected in all of our samples and showed a trend of increased abundance in HD RNA granules and a decreased abundance in HD sEVs. This difference in abundance between our cell model and the study by Neueder et al. may be explained by the fact that EVs isolated from blood are derived from diverse body cell types, mostly from platelets. The study by Neueder et al. revealed a high expression of many deregulated proteins in liver indicating that liver may be the main source of the observed changes in EV protein content and composition [37]. Thus, these gene patterns may not be reflected in HEK cells originating from kidney.

When comparing our list of marker genes with a list of the top 20 differentially expressed genes in HD across ten categories [45], we found two matches: *PLCB1* and *CDH10*. While our data showed *PLCB1* to be enriched under HD conditions in sEVs, this gene was reported being down-regulated in HD [46]. This may be explained by the fact that we analyzed the content of sEV-secreted transcripts, while the other studies analyzed the intracellular transcript levels.

Both *HTT* protein and RNA are secreted via EVs [21,70]. Moreover, HEK293 T cells overexpressing mutant *HTT*-GFP fusion constructs release EVs containing the mutant *HTT* protein and its encoding RNA [71]. In line with these data, *HTT* was detected in all our samples. Our quantitative analysis showed a trend of increased abundance in HD RNA granules and a decreased abundance in HD sEVs. Thus, our data suggest that mutant *HTT* may be stored intracellularly in RNA granules but may not be preferentially sorted into sEVs.

Generally, RNA granules that form upon arsenite treatment (stress granules) contain both cytosolic proteins and RNAs, with proportionally more RNAs than proteins inside stress granule compared to the cytoplasm [72,73]. In line with our transcriptomic analysis of RNA granule cores that formed upon arsenite treatment, different RNA species are known to localize into stress granules including mRNAs and lncRNAs [74]. While both mRNA and ncRNAs can be targeted to stress granules, their targeting efficiency varies from <1 % to >95 % [73]. In line with this, our localization studies of the HD marker transcripts showed that the three transcripts we tested only partially localized to intracellular RNA granules that formed upon cell stress, but a considerable fraction

was still detected in the cytoplasm outside the RNA granules.

5. Conclusions

Taken together, our study describes the first systematic analysis of sEVs and RNA granules in an HD cell model. Our data points towards a connection between intracellular RNA granules and sEVs and the importance of lncRNAs in RNA granule formation (Fig. 8). Moreover, our results suggest that lncRNAs may serve as HD markers. However, our qPCR validation experiments showed that there is a high variability in technical and biological replicates in analysis of sEV cargo. This should be considered as a limitation for the use of sEVs as diagnostic markers. In line with this notion, a study of sEVs secreted from platelets from HD patients at different stages of the disease showed that platelets do not secrete sEVs containing valuable biomarker [75]. Further studies are important to understand, highlight and establish the role of these lncRNAs in the disease state.

CRedit authorship contribution statement

Deepti Kailash Nabariya: Writing – original draft, Visualization, Methodology, Investigation. **Lisa Maria Knüpfner:** Methodology, Investigation. **Patrick Hartwich:** Methodology, Investigation. **Manuela S. Killian:** Methodology, Investigation. **Florian Centler:** Visualization, Methodology, Investigation, Formal analysis. **Sybille Krauß:** Writing – original draft, Supervision, Methodology, Investigation, Formal analysis, Conceptualization.

Declaration of competing interest

The authors declare no conflict of interest.

Acknowledgments

We thank Prof. Erich Wanker for providing the HEKQ83 cell line. We thank Andre Hossinger and Ina Vorberg for supporting the NTA analysis. We thank Dr. Christian Pritzel for assistance in SEM measurements. Part of this work was conducted at MNAF Siegen. We thank Andreas Neueder for sharing raw sequencing data from patient plasma extracellular vesicles prior to publication (now published).

This work was supported by the DFG Major Research Instrumentation Programme (INST 221/145-1 FUGG). This work was supported by the DFG Research Infrastructure NGS_CC (project 407495230) as part of the Next Generation Sequencing Competence Network (project 423957469). NGS analyses were carried out at the Competence Centre for Genomic Analysis (Kiel).

Appendix A. Supplementary data

Supplementary data to this article can be found online at <https://doi.org/10.1016/j.mcp.2025.102026>.

Data availability

Raw RNAseq data and salmon output are available from Gene Expression Omnibus (GEO accession: GSE261143).

References

- [1] J.B. Carroll, G.P. Bates, J. Steffan, C. Saft, S.J. Tabrizi, Treating the whole body in Huntington's disease, *Lancet Neurol.* 14 (11) (2015) 1135–1142, [https://doi.org/10.1016/S1474-4422\(15\)00177-5](https://doi.org/10.1016/S1474-4422(15)00177-5).
- [2] D.R. Schoenberg, L.E. Maquat, Regulation of cytoplasmic mRNA decay, *Nat. Rev. Genet.* 13 (4) (2012) 246–259, <https://doi.org/10.1038/nrg3160>.
- [3] H. An, C.R. de Meritens, T.A. Shelkovernikova, Connecting the "dots": RNP granule network in health and disease, *Biochim. Biophys. Acta Mol. Cell Res.* 1868 (8) (2021) 119058, <https://doi.org/10.1016/j.bbamcr.2021.119058>.

- [4] P. Anderson, N. Kedersha, RNA granules, *J. Cell Biol.* 172 (6) (2006) 803–808, <https://doi.org/10.1083/jcb.200512082>.
- [5] P. Anderson, N. Kedersha, RNA granules: post-transcriptional and epigenetic modulators of gene expression, *Nat. Rev. Mol. Cell Biol.* 10 (6) (2009) 430–436, <https://doi.org/10.1038/nrm2694>.
- [6] J.R. Buchan, R. Parker, Eukaryotic stress granules: the ins and outs of translation, *Mol Cell* 36 (6) (2009) 932–941, <https://doi.org/10.1016/j.molcel.2009.11.020>.
- [7] A.C. Fan, A.K. Leung, RNA granules and diseases: a case study of stress granules in ALS and FTL, *Adv. Exp. Med. Biol.* 907 (2016) 263–296, https://doi.org/10.1007/978-3-319-29073-7_11.
- [8] C.J. Decker, R. Parker, P-bodies and stress granules: possible roles in the control of translation and mRNA degradation, *Cold Spring Harbor Perspect. Biol.* 4 (9) (2012) a012286, <https://doi.org/10.1101/cshperspect.a012286>.
- [9] O. Moujaber, U. Stochaj, Cytoplasmic RNA granules in somatic maintenance, *Gerontology* 64 (5) (2018) 485–494, <https://doi.org/10.1159/000488759>.
- [10] D.L. Spector, SnapShot: cellular bodies, *Cell* 127 (5) (2006) 1071, <https://doi.org/10.1016/j.cell.2006.11.026>.
- [11] M. de Mezer, M. Wojciechowska, M. Napierala, K. Sobczak, W.J. Krzyzosiak, Mutant CAG repeats of Huntingtin transcript fold into hairpins, form nuclear foci and are targets for RNA interference, *Nucleic Acids Res.* 39 (9) (2011) 3852–3863, <https://doi.org/10.1093/nar/gkq1323>.
- [12] I.I. Sanchez, T.B. Nguyen, W.E. England, R.G. Lim, A.Q. Vu, R. Miramontes, L. M. Thompson, Huntington's disease mice and human brain tissue exhibit increased G3BP1 granules and TDP43 mislocalization, *J. Clin. Investig.* 131 (12) (2021), <https://doi.org/10.1172/jci140723>.
- [13] J.N. Savas, A. Makusky, S. Ottosen, D. Baillat, F. Then, D. Krainc, N. Tanese, Huntington's disease protein contributes to RNA-mediated gene silencing through association with Argonaute and P bodies, *Proc. Natl. Acad. Sci. U. S. A.* 105 (31) (2008) 10820–10825, <https://doi.org/10.1073/pnas.0800658105>.
- [14] J.A. Welsh, D.C.I. Goberdhan, L. O'Driscoll, E.I. Buzas, C. Blenkinsop, B. Bussolati, K.W. Witwer, Minimal information for studies of extracellular vesicles (MISEV2023): from basic to advanced approaches, *J. Extracell. Vesicles* 13 (2) (2024) e12404, <https://doi.org/10.1002/jev2.12404>.
- [15] D. Xie, B. Qian, X. Li, Nucleic acids and proteins carried by exosomes from various sources: potential role in liver diseases, *Front. Physiol.* 13 (2022) 957036, <https://doi.org/10.3389/fphys.2022.957036>.
- [16] A.F. Hill, Extracellular vesicles and neurodegenerative diseases, *J. Neurosci.* 39 (47) (2019) 9269–9273, <https://doi.org/10.1523/JNEUROSCI.0147-18.2019>.
- [17] C. Masdeu, H. Faure, J. Coulombe, A. Schoenfelder, A. Mann, I. Brabet, M. Ruat, Identification and characterization of Hedgehog modulator properties after functional coupling of Smoothened to G15, *Biochem. Biophys. Res. Commun.* 349 (2) (2006) 471–479, <https://doi.org/10.1016/j.bbrc.2006.07.216>.
- [18] S. Wang, F. Cesca, G. Loers, M. Schweizer, F. Buck, F. Benfenati, R. Kleene, Synapsin I is an oligomannose-carrying glycoprotein, acts as an oligomannose-binding lectin, and promotes neurite outgrowth and neuronal survival when released via glia-derived exosomes, *J. Neurosci.* 31 (20) (2011) 7275–7290, <https://doi.org/10.1523/JNEUROSCI.6476-10.2011>.
- [19] E.M. Kramer-Albers, N. Bretz, S. Tenzer, C. Winterstein, W. Mobius, H. Berger, J. Trotter, Oligodendrocytes secrete exosomes containing major myelin and stress-protective proteins: trophic support for axons? *Proteomics Clin. Appl.* 1 (11) (2007) 1446–1461, <https://doi.org/10.1002/prca.200700522>.
- [20] Y. Hong, T. Zhao, X.J. Li, S. Li, Mutant huntingtin inhibits alphaB-crystallin expression and impairs exosome secretion from astrocytes, *J. Neurosci.* 37 (39) (2017) 9550–9563, <https://doi.org/10.1523/JNEUROSCI.1418-17.2017>.
- [21] H. Ananbeh, J. Novak, S. Juhas, J. Juhasova, J. Klempir, K. Doleckova, H. Kupcova Skalinikova, Huntingtin Co-isolates with small extracellular vesicles from blood plasma of TgHD and KI-HD pig models of huntingtin's disease and human blood plasma, *Int. J. Mol. Sci.* 23 (10) (2022), <https://doi.org/10.3390/ijms23105598>.
- [22] X. Zhang, E.R. Abels, J.S. Redzic, J. Margulis, S. Finkbeiner, X.O. Breakefield, Potential transfer of polyglutamine and CAG-repeat RNA in extracellular vesicles in huntingtin's disease: background and evaluation in cell culture, *Cell. Mol. Neurobiol.* 36 (3) (2016) 459–470, <https://doi.org/10.1007/s10571-016-0350-7>.
- [23] I. Jeon, F. Cicchetti, G. Cisbani, S. Lee, E. Li, J. Bae, J. Song, Human-to-mouse prion-like propagation of mutant huntingtin protein, *Acta Neuropathol.* 132 (4) (2016) 577–592, <https://doi.org/10.1007/s00401-016-1582-9>.
- [24] A.M. Leidal, H.H. Huang, T. Marsh, T. Solvik, D. Zhang, J. Ye, J. Debnath, The LC3-conjugation machinery specifies the loading of RNA-binding proteins into extracellular vesicles, *Nat. Cell Biol.* 22 (2) (2020) 187–199, <https://doi.org/10.1038/s41556-019-0450-y>.
- [25] X.M. Liu, L. Ma, R. Schekman, Selective sorting of microRNAs into exosomes by phase-separated YBX1 condensates, *Elife* 10 (2021), <https://doi.org/10.7554/eLife.71982>.
- [26] S. Markmiller, S. Soltanieh, K.L. Server, R. Mak, W. Jin, M.Y. Fang, G.W. Yeo, Context-Dependent and disease-specific diversity in protein interactions within stress granules, *Cell* 172 (3) (2018), <https://doi.org/10.1016/j.cell.2017.12.032>, 590–604 e513.
- [27] D.K. Nabariya, A. Heinz, S. Derksen, S. Krauss, Intracellular and intercellular transport of RNA organelles in CXG repeat disorders: the strength of weak ties, *Front. Mol. Biosci.* 9 (2022) 1000932, <https://doi.org/10.3389/fmolb.2022.1000932>.
- [28] S. Waelter, A. Boeddrich, R. Lurz, E. Scherzinger, G. Lueder, H. Lehrach, E. E. Wanker, Accumulation of mutant huntingtin fragments in aggresome-like inclusion bodies as a result of insufficient protein degradation, *Mol. Biol. Cell* 12 (5) (2001) 1393–1407. Retrieved from, http://www.ncbi.nlm.nih.gov/entrez/quer.fcgi?cmd=Retrieve&db=PubMed&dopt=Citation&list_uids=11359930.
- [29] G. Raposo, H.W. Nijman, W. Stoorvogel, R. Liejendekker, C.V. Harding, C.J. Melief, H.J. Geuze, B lymphocytes secrete antigen-presenting vesicles, *J. Exp. Med.* 183 (3) (1996) 1161–1172, <https://doi.org/10.1084/jem.183.3.1161>.
- [30] H. Lee, D. Zhang, Z. Zhu, C.S. Dela Cruz, Y. Jin, Epithelial cell-derived microvesicles activate macrophages and promote inflammation via microvesicle-containing microRNAs, *Sci. Rep.* 6 (2016) 35250, <https://doi.org/10.1038/srep35250>.
- [31] S. Namkoong, A. Ho, Y.M. Woo, H. Kwak, J.H. Lee, Systematic characterization of stress-induced RNA granulation, *Mol Cell* 70 (1) (2018) 175–187.e178, <https://doi.org/10.1016/j.molcel.2018.02.025>.
- [32] C. Thery, K.W. Witwer, E. Aikawa, M.J. Alcaraz, J.D. Anderson, R. Andriantsohaina, E.K. Zuba-Surma, Minimal information for studies of extracellular vesicles 2018 (MISEV2018): a position statement of the International Society for Extracellular Vesicles and update of the MISEV2014 guidelines, *J. Extracell. Vesicles* 7 (1) (2018) 1535750, <https://doi.org/10.1080/20013078.2018.1535750>.
- [33] A.M. Bolger, M. Lohse, B. Usadel, Trimmomatic: a flexible trimmer for Illumina sequence data, *Bioinformatics* 30 (15) (2014) 2114–2120, <https://doi.org/10.1093/bioinformatics/btu170>.
- [34] M. Martin, Cutadapt removes adapter sequences from high-throughput sequencing reads, *EMBnet.journal* 17 (1) (2011) 10–12, <https://doi.org/10.14806/ej.17.1.200>.
- [35] R. Patro, G. Duggal, M.I. Love, R.A. Irizarry, C. Kingsford, Salmon provides fast and bias-aware quantification of transcript expression, *Nat. Methods* 14 (4) (2017) 417–419, <https://doi.org/10.1038/nmeth.4197>.
- [36] C. Sonesson, M.I. Love, M.D. Robinson, Differential analyses for RNA-seq: transcript-level estimates improve gene-level inferences, *F1000Res* 4 (2015) 1521, <https://doi.org/10.12688/f1000research.7563.2>.
- [37] A. Neueder, P. Nitzschner, R. Wagner, J. Hummel, F. Hoschek, M. Wagner, M. Orth, Huntington disease alters the actionable information in plasma extracellular vesicles, *Clin. Transl. Med.* 14 (1) (2024) e1525, <https://doi.org/10.1002/ctm2.1525>.
- [38] M.I. Love, W. Huber, S. Anders, Moderated estimation of fold change and dispersion for RNA-seq data with DESeq2, *Genome Biol.* 15 (12) (2014) 550, <https://doi.org/10.1186/s13059-014-0550-8>.
- [39] M. Stephens, False discovery rates: a new deal, *Biostatistics* 18 (2) (2017) 275–294, <https://doi.org/10.1093/biostatistics/kwx041>.
- [40] D. Szklarczyk, R. Kirsch, M. Koutrouli, K. Nastou, F. Mehryary, R. Hachilif, C. von Mering, The STRING database in 2023: protein-protein association networks and functional enrichment analyses for any sequenced genome of interest, *Nucleic Acids Res.* 51 (D1) (2023) D638–d646, <https://doi.org/10.1093/nar/gkac1000>.
- [41] S.A. Aleksander, J. Balhoff, S. Carbon, J.M. Cherry, H.J. Drabkin, D. Ebert, M. Westerfield, The gene ontology knowledgebase in 2023, *Genetics* 224 (1) (2023), <https://doi.org/10.1093/genetics/iyad031>.
- [42] M. Ashburner, C.A. Ball, J.A. Blake, D. Botstein, H. Butler, J.M. Cherry, G. Sherlock, Gene ontology: tool for the unification of biology. The Gene Ontology Consortium, *Nat. Genet.* 25 (1) (2000) 25–29, <https://doi.org/10.1038/75556>.
- [43] J.A. Batsis, G.G. Boateng, L.M. Seo, C.L. Petersen, K.L. Fortuna, E.V. Wechsler, D. F. Kotz, Development and usability assessment of a connected resistance exercise band application for strength-monitoring, *World Acad Sci Eng Technol* 13 (5) (2019) 340–348, <https://doi.org/10.5281/zenodo>.
- [44] O. Liska, B. Bohár, A. Hidas, T. Korcsmáros, B. Papp, D. Fazekas, E. Ari, TFLink: an integrated gateway to access transcription factor-target gene interactions for multiple species, *Database* 2022 (2022), <https://doi.org/10.1093/database/baac083>.
- [45] B. Malla, X. Guo, G. Senger, Z. Chasapopoulou, F. Yildirim, A systematic review of transcriptional dysregulation in huntingtin's disease studied by RNA sequencing, *Front. Genet.* 12 (2021) 751033, <https://doi.org/10.3389/fgene.2021.751033>.
- [46] A. Kuhn, D.R. Goldstein, A. Hodges, A.D. Strand, T. Sengstag, C. Kooperberg, R. Luthi-Carter, Mutant huntingtin's effects on striatal gene expression in mice recapitulate changes observed in human Huntington's disease brain and do not differ with mutant huntingtin length or wild-type huntingtin dosage, *Hum. Mol. Genet.* 16 (15) (2007) 1845–1861, <https://doi.org/10.1093/hmg/ddm133>.
- [47] Y.N. Jin, G.V. Johnson, The interrelationship between mitochondrial dysfunction and transcriptional dysregulation in Huntington disease, *J. Bioenerg. Biomembr.* 42 (3) (2010) 199–205, <https://doi.org/10.1007/s10863-010-9286-7>.
- [48] A. Medina, Y. Mahjoub, L. Shaver, T. Pringsheim, Prevalence and incidence of huntingtin's disease: an updated systematic review and meta-analysis, *Mov. Disord.* 37 (12) (2022) 2327–2335, <https://doi.org/10.1002/mds.29228>.
- [49] M. Mo, Editorial: non-coding RNAs in neurodegenerative diseases, *Front. Neurosci.* 17 (2023) 1241737, <https://doi.org/10.3389/fnins.2023.1241737>.
- [50] M. Serpente, C. Fenoglio, M. D'Anca, M. Arcaro, F. Sorrentino, C. Visconte, D. Galimberti, MiRNA profiling in plasma neural-derived small extracellular vesicles from patients with Alzheimer's disease, *Cells* 9 (6) (2020), <https://doi.org/10.3390/cells9061443>.
- [51] L. Zhao, Y. Ye, L. Gu, Z. Jian, C.M. Stary, X. Xiong, Extracellular vesicle-derived miRNA as a novel regulatory system for bi-directional communication in gut-brain-microbiota axis, *J. Transl. Med.* 19 (1) (2021) 202, <https://doi.org/10.1186/s12967-021-02861-y>.
- [52] M. Huarte, M. Guttman, D. Feldser, M. Garber, M.J. Kozio, D. Kenzelmann-Broz, J. L. Rinn, A large intergenic noncoding RNA induced by p53 mediates global gene repression in the p53 response, *Cell* 142 (3) (2010) 409–419, <https://doi.org/10.1016/j.cell.2010.06.040>.
- [53] I.J. Matouk, N. DeGroot, S. Mezan, S. Ayes, R. Abu-lail, A. Hochberg, E. Galun, The H19 non-coding RNA is essential for human tumor growth, *PLoS One* 2 (9) (2007) e845, <https://doi.org/10.1371/journal.pone.0000845>.

- [54] J.R. Prensner, M.K. Iyer, O.A. Balbin, S.M. Dhanasekaran, Q. Cao, J.C. Brenner, A. M. Chinnaiyan, Transcriptome sequencing across a prostate cancer cohort identifies PCAT-1, an unannotated lincRNA implicated in disease progression, *Nat. Biotechnol.* 29 (8) (2011) 742–749, <https://doi.org/10.1038/nbt.1914>.
- [55] M. Zhang, P. He, Z. Bian, Long noncoding RNAs in neurodegenerative diseases: pathogenesis and potential implications as clinical biomarkers, *Front. Mol. Neurosci.* 14 (2021) 685143, <https://doi.org/10.3389/fnmol.2021.685143>.
- [56] L. Lipovich, F. Datchet, J. Cai, S. Bagla, K. Balan, H. Jia, J.A. Loeb, Activity-dependent human brain coding/noncoding gene regulatory networks, *Genetics* 192 (3) (2012) 1133–1148, <https://doi.org/10.1534/genetics.112.145128>.
- [57] M. Shimojo, Huntingtin regulates RE1-silencing transcription factor/neuron-restrictive silencer factor (REST/NRSF) nuclear trafficking indirectly through a complex with REST/NRSF-interacting LIM domain protein (RILP) and dynactin p150 Glued, *J. Biol. Chem.* 283 (50) (2008) 34880–34886, <https://doi.org/10.1074/jbc.M804183200>.
- [58] C. Zuccato, M. Tartari, A. Crotti, D. Goffredo, M. Valenza, L. Conti, E. Cattaneo, Huntingtin interacts with REST/NRSF to modulate the transcription of NRSE-controlled neuronal genes, *Nat. Genet.* 35 (1) (2003) 76–83, <https://doi.org/10.1038/ng1219>.
- [59] R. Johnson, N. Richter, R. Jauch, P.M. Gaughwin, C. Zuccato, E. Cattaneo, L. W. Stanton, Human accelerated region 1 noncoding RNA is repressed by REST in Huntington's disease, *Physiol. Genom.* 41 (3) (2010) 269–274, <https://doi.org/10.1152/physiolgenomics.00019.2010>.
- [60] R. Johnson, Long non-coding RNAs in Huntington's disease neurodegeneration, *Neurobiol. Dis.* 46 (2) (2012) 245–254, <https://doi.org/10.1016/j.nbd.2011.12.006>.
- [61] P. Johnsson, L. Lipovich, D. Grandér, K.V. Morris, Evolutionary conservation of long non-coding RNAs; sequence, structure, function, *Biochim. Biophys. Acta* 1840 (3) (2014) 1063–1071, <https://doi.org/10.1016/j.bbagen.2013.10.035>.
- [62] L. Smeenk, S.J. van Heeringen, M. Koeppl, B. Gilbert, E. Janssen-Megens, H. G. Stunnenberg, M. Lohrum, Role of p53 serine 46 in p53 target gene regulation, *PLoS One* 6 (3) (2011) e17574, <https://doi.org/10.1371/journal.pone.0017574>.
- [63] J.S. Sunwoo, S.T. Lee, W. Im, M. Lee, J.I. Byun, K.H. Jung, M. Kim, Altered expression of the long noncoding RNA NEAT1 in huntington's disease, *Mol. Neurobiol.* 54 (2) (2017) 1577–1586, <https://doi.org/10.1007/s12035-016-9928-9>.
- [64] F. Cherbonneau, G. Li, P. Gokulnath, P. Sahu, A. Prunevieuille, R. Kitchen, S. Das, TRACE-seq: a transgenic system for unbiased and non-invasive transcriptome profiling of living cells, *iScience* 25 (2) (2022) 103806, <https://doi.org/10.1016/j.isci.2022.103806>.
- [65] U. Gezer, E. Özgür, M. Cetinkaya, M. Isin, N. Dalay, Long non-coding RNAs with low expression levels in cells are enriched in secreted exosomes, *Cell Biol. Int.* 38 (9) (2014) 1076–1079, <https://doi.org/10.1002/cbin.10301>.
- [66] L. Mangiarini, K. Sathasivam, M. Sellar, B. Cozens, A. Harper, C. Hetherington, G. P. Bates, Exon 1 of the HD gene with an expanded CAG repeat is sufficient to cause a progressive neurological phenotype in transgenic mice, *Cell* 87 (3) (1996) 493–506, [https://doi.org/10.1016/s0092-8674\(00\)81369-0](https://doi.org/10.1016/s0092-8674(00)81369-0).
- [67] A. Neueder, C. Landles, R. Ghosh, D. Howland, R.H. Myers, R.L.M. Faull, G. P. Bates, The pathogenic exon 1 HTT protein is produced by incomplete splicing in Huntington's disease patients, *Sci. Rep.* 7 (1) (2017) 1307, <https://doi.org/10.1038/s41598-017-01510-z>.
- [68] K. Sathasivam, A. Neueder, T.A. Gipson, C. Landles, A.C. Benjamin, M. K. Bondulich, G.P. Bates, Aberrant splicing of HTT generates the pathogenic exon 1 protein in Huntington disease, *Proc. Natl. Acad. Sci. U. S. A.* 110 (6) (2013) 2366–2370, <https://doi.org/10.1073/pnas.1221891110>.
- [69] R. Gutierrez-Garcia, S. Koyuncu, F. Hommen, S. Bilican, H.J. Lee, A. Fatima, D. Vilchez, G3BP1-dependent mechanism suppressing protein aggregation in Huntington's models and its demise upon stress granule assembly, *Hum. Mol. Genet.* 32 (10) (2023) 1607–1621, <https://doi.org/10.1093/hmg/ddac304>.
- [70] D. Pink, J. Donnelier, J.D. Lewis, J.E.A. Braun, Cysteine string protein controls two routes of export for misfolded huntingtin, *Front. Neurosci.* 15 (2021) 762439, <https://doi.org/10.3389/fnins.2021.762439>.
- [71] J. Zhang, S. Wang, F. Han, J. Li, L. Yu, P. Zhou, Q. Li, MicroRNA-542-3p suppresses cellular proliferation of bladder cancer cells through post-transcriptionally regulating survivin, *Gene* 579 (2) (2016) 146–152, <https://doi.org/10.1016/j.gene.2015.12.048>.
- [72] O. Bounedjah, B. Desforges, T.D. Wu, C. Pioche-Durieu, S. Marco, L. Hamon, D. Pastré, Free mRNA in excess upon polysome dissociation is a scaffold for protein multimerization to form stress granules, *Nucleic Acids Res.* 42 (13) (2014) 8678–8691, <https://doi.org/10.1093/nar/gku582>.
- [73] A. Khong, T. Matheny, S. Jain, S.F. Mitchell, J.R. Wheeler, R. Parker, The stress granule transcriptome reveals principles of mRNA accumulation in stress granules, *Mol Cell* 68 (4) (2017), <https://doi.org/10.1016/j.molcel.2017.10.015>, 808–820 e805.
- [74] D. Campos-Melo, Z.C.E. Hawley, C.A. Droppelmann, M.J. Strong, The integral role of RNA in stress granule formation and function, *Front. Cell Dev. Biol.* 9 (2021) 621779, <https://doi.org/10.3389/fcell.2021.621779>.
- [75] H.L. Denis, J. Lamontagne-Proulx, I. St-Amour, S.L. Mason, A. Weiss, S. Chouinard, F. Cicchetti, Platelet-derived extracellular vesicles in Huntington's disease, *J. Neurol.* 265 (11) (2018) 2704–2712, <https://doi.org/10.1007/s00415-018-9022-5>.